Coexistence of the δl and δT_c flux pinning mechanisms in nano-Si-doped MgB$_2$

S R Ghorbani[1,2], **X L Wang**[1], **M S A Hossain**[1], **S X Dou**[1] and **Sung-Ik Lee**[3]

[1] Institute for Superconducting and Electronic Materials, University of Wollongong, Wollongong, New South Wales 2522, Australia
[2] Department of Physics, Sabzevar Tarbiat Moallem University, PO Box 397, Sabzevar, Iran
[3] National Creative Research Initiative Center for Superconductivity, Department of Physics, Sogang University, Seoul 121-742, Republic of Korea

E-mail: xiaolin@uow.edu.au and silee77@sogang.ac.kr

Abstract

The flux pinning mechanisms of nano-Si-doped MgB$_2$ are reported in this work. The field dependence of the critical current density, $J_c(B)$, was analyzed within the collective pinning model. We found that the mechanisms for both δl pinning, i.e., pinning associated with charge-carrier mean free path fluctuations, and δT_c pinning, which is associated with spatial fluctuations of the transition temperature, coexist in the nano-Si-doped MgB$_2$ samples, while H_{c2} increases greatly with increasing nano-Si doping level. However, their contributions are strongly temperature dependent. The δl pinning is dominant at low temperatures, decreases with increasing temperature, and is suppressed completely at temperatures close to the critical temperature, T_c. However, the δT_c pinning mechanism shows opposite trends.

(Some figures in this article are in colour only in the electronic version)

1. Introduction

The upper critical field, H_{c2}, in MgB$_2$ can be significantly enhanced using various approaches, including high energy ion irradiation [1], chemical substitution, and incorporation of nanoparticles such as nano-SiC, C, Si, and other oxide or non-oxide nanomaterials [2–13]. It has been accepted that enhancement of H_{c2} is caused by C substitution for B in the crystal lattice as a result of chemical doping that contains C. The mean free path, l, is reduced due to distortion in the lattice caused by the C substitution. Therefore, the σ band electron scattering is enhanced, leading to an increase in H_{c2} and a large decrease in T_c, which is a disadvantage for applications at $T > 20$ K. It should be noted that H_{c2} can still be enhanced in MgB$_2$ doped with non-carbon nanoparticles, even though there are no substitution effects. Nano-Si has been found to be very effective for improving the critical current density, J_c, in both low and high fields, with only a slight reduction in the critical temperature, T_c, although no Si substitution takes place [8, 9]. The J_c values at temperatures above 20 K for nano-Si-doped MgB$_2$ were found to be even higher than that of C-doped MgB$_2$ [8, 9]. However, the flux pinning mechanism for the nano-Si-doped MgB$_2$ has not been studied so far.

The irreversibility field, H_{irr}, and the in-field J_c are mainly controlled by flux pinning. Numerous studies have been performed with the purpose of understanding the vortex pinning mechanisms [14–22] that are responsible for improving the J_c. Inter-grain boundary pinning [20] and point defect pinning [17] are the two main important pinning mechanisms. The inclusion of nano-Si can introduce pinning centers without any substitution effects [23, 24]. This provides an advantage in understanding the flux pinning mechanism compared to the nano-C dopants, which can contribute all the effects of point defects, grain boundaries, and substitution to the flux pinning in MgB$_2$. Therefore, the pinning mechanisms are of great interest in nano-Si-doped MgB$_2$ from the point of view of both the fundamental physics and applications.

It is believed that fluctuations in both T_c and the mean free path of charge carriers control the flux pinning in high T_c superconductors [25, 26]. The T_c fluctuation in MgB$_2$ is due to Mg deficiency and partial dopant substitution into the lattice, which lead to a broad T_c distribution in the sample [24]. However, it is the inter-grain boundaries and the nanoparticle inclusions inside the MgB$_2$ grains that cause the mean free path fluctuations and hence the δl pinning. It has been reported that

the δT_c pinning is the main flux pinning mechanism in pure MgB$_2$ bulk and thin films [18, 27, 28]. However, it has not been experimentally determined whether the δT_c pinning or the δl pinning is the dominant mechanism in doped MgB$_2$.

In this paper the vortex pinning mechanisms of the nano-Si-doped samples are discussed in the framework of the collective theory. It was found that both the δl and δT_c pinning mechanisms coexist in the nano-Si-doped MgB$_2$ samples. Their contributions are strongly temperature dependent and show a strong competition.

2. Experimental procedure

Polycrystalline MgB$_2$ samples doped with 2 and 5 wt% nano-Si powders were prepared with the same conditions using the *in situ* solid state reaction [8, 9]. Magnesium powders and amorphous boron powders were well mixed with silicon powders with particle sizes <100 nm. Pellets 10 mm in diameter and 1 mm in thickness were made under pressure, and sealed in Fe tubes, then heat treated at 700 °C for 30 min in flowing high purity Ar. This was followed by a furnace cooling to room temperature. The x-ray diffraction (XRD) and the transmission electron microscopy (TEM) results revealed that all the samples were crystallized in the MgB$_2$ structure as the major phase. A few impurity lines from MgO and Mg$_2$Si were observed. The TEM image of MgB$_2$ grains from a nano-Si-doped MgB$_2$ sample showed a number of fine grains, around 100–200 nm in diameter. Most of these were shown by electron diffraction to be MgB$_2$. But a number of grains, 10–30 nm in size located on the MgB$_2$ grains, were determined by electron diffraction to be Mg$_2$Si [8].

The resistivity measurements were carried out on bare cylindrical bar samples by using a physical properties measurement system (PPMS, Quantum Design) in the field range from 0 up to 8.7 T. The magnetic hysteresis loops were measured using a magnetic properties measurement system (MPMS, Quantum Design). The critical current density was calculated by using the Bean approximation.

3. Results and discussion

The phases and microstructures examined by XRD and TEM show that Mg$_2$Si is the main impurity phase and that the particle sizes of the MgB$_2$ are almost the same for all the samples [8, 9]. It was observed that the resistivity of the nano-Si-doped samples increases with increasing silicon concentration (see the inset of figure 1(a)). The resistivity is about 24.2 and 104.2 $\mu\Omega$ cm at 300 K, and 13.2 and 53.5 $\mu\Omega$ cm at 40 K for the 2 and 5 wt% Si-doped MgB$_2$ samples, respectively. The residual resistivity ratio RRR = ρ(300 K)/ρ(40 K) = 1.83 and 1.95 for the 2 and 5 wt% Si samples, respectively. The increase in the resistivity is pronounced as the temperature approaches the transition temperature, indicating enhanced electron scattering, which is similar to the case for C-doped MgB$_2$. The T_c of the 2 and 5 wt% Si-doped MgB$_2$ samples are 37.5 and 36.7 K, respectively, which is slightly lower than that of the undoped
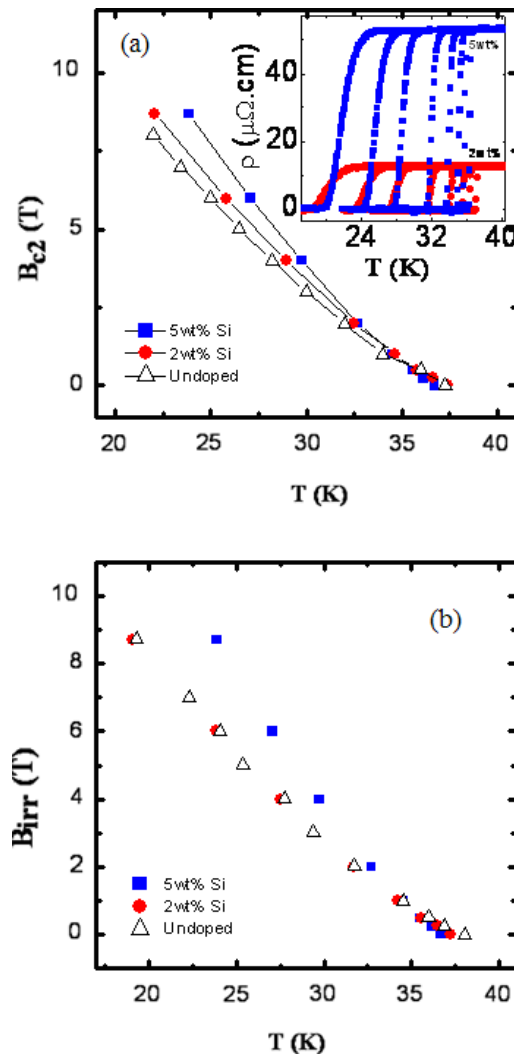

Figure 1. (a) B_{c2} and (b) B_{irr} versus temperature for the 2 and 5 wt% nano-Si-doped MgB$_2$. The inset in (a) shows ρ–T in fields up to 8.7 T for both samples.

sample (38.0 K). The small drop in the T_c for the nano-Si-doped sample is caused by both Mg deficiency as a result of the formation of Mg$_2$Si and the enhanced electron scattering from the Mg$_2$Si impurity. The mean free path, l, was calculated using the mean value of the Fermi velocity v_F = 5.1 $\times$ 10^5 m s^{-1} [29] and the resistivity at 40 K. It decreases from 1.03 nm for 2 wt% Si doping to 0.24 nm for 5 wt% Si doping, which is in good agreement with the observed enhancement in H_{c2}.

The H_{c2} and H_{irr} for both nano-Si-doped MgB$_2$ samples were defined as H_{c2} = 0.9$R(T_c)$ and H_{irr} = 0.1$R(T_c)$ from the resistance (R) versus temperature (T) curve. The temperature dependences of H_{irr} and H_{c2} are shown in figure 1. It can be seen that the H_{c2} values for the doped samples are proportional to the Si doping level and are higher than for the undoped sample. For the 5 wt% nano-Si-doped MgB$_2$, the H_{irr} is higher than for both the undoped and the 2 wt% doped MgB$_2$. However, the H_{irr} of the 2 wt% Si-doped sample is the same as that of the undoped one, indicating that the H_{irr} does not necessarily increase when the H_{c2} increases. This is an indication that the H_{irr} is mainly controlled by the flux pinning.
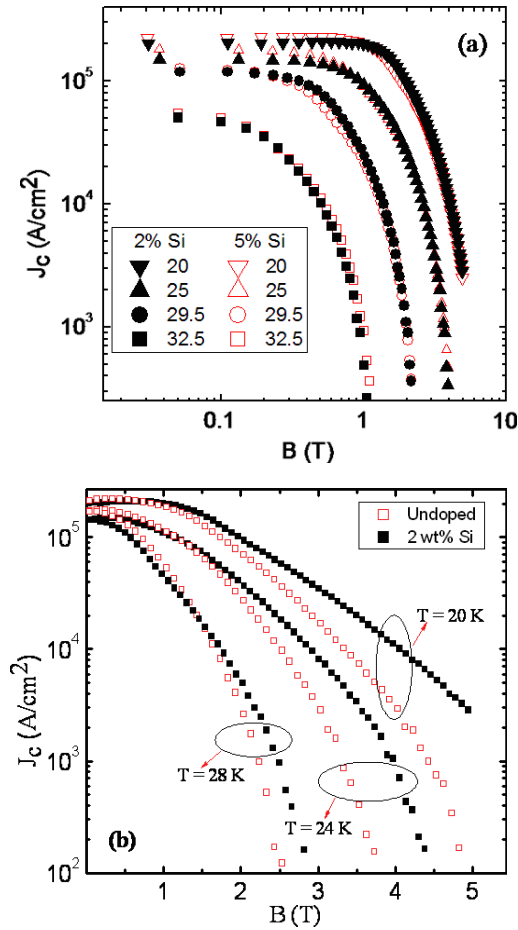
Figure 2. Field dependence of J_c for the 2 and 5 wt% nano-Si-doped MgB_2 (a) and for the undoped and 2 wt% nano-Si-doped MgB_2 (b).

The $J_c(B, T)$ results for nano-Si-doped samples are shown in a double-logarithmic plot in figure 2(a). The J_c at 20 K is over 2×10^5 A cm^{-2} at zero field and over 1×10^4 A cm^{-2} at 4 T for both doped samples. It can also been seen that the 5 wt% Si-doped sample shows lower J_c for 1 T $< B <$ 3 T at $T = 20$ K. The J_c values in high fields ($B > 3$ T) are the same for both samples. In addition, for $T > 25$ K, the J_c values are almost independent of the Si content. The J_c values of the undoped sample and of the 2 wt% Si-doped sample are compared in figure 2(b) at 20, 24, and 28 K. As can be seen from this figure, the J_c is very much enhanced in high magnetic fields for the Si-doped MgB_2, and it is more than 10 times higher than for the undoped MgB_2 at $T = 20$ K and $B = 5$ T. Therefore, the nano-Si-doped MgB_2 exhibits significantly improved pinning in high fields over a wide temperature range compared with the undoped MgB_2 sample. In low magnetic fields, however, the J_c of the nano-Si-doped samples is lower than that of the undoped sample. These results suggest that the formation of Mg_2Si impurities is responsible for two effects. The first one is that the amount of MgB_2 phase is accordingly decreased, which decreases the effective superconducting volume inside the nano-Si-doped samples. This effect results in decreased J_c in low fields. The second effect is the formation of nanosized pinning centers, which improves J_c–H behavior in high magnetic fields. This result is in agreement with what we have reported before [8, 9].
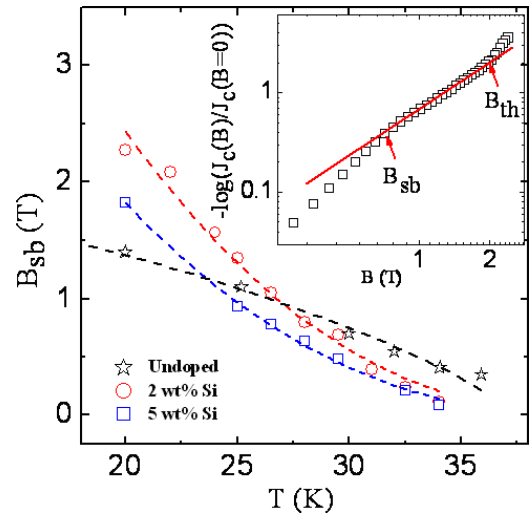

Figure 3. B_{sb} versus T. The dashed curves are fits to the $B_{sb} = P_1 B_{sb}^{T_c} + P_2 B_{sb}^{l}$ expression. Inset: double-logarithmic plot of $-\log[J_c(B)/J_c(0)]$ versus B at $T = 29.5$ K for the 2 wt% Si-doped sample. The data for the undoped sample are extracted from [30].

In the framework of the collective theory [26], B_{sb} is defined as the crossover field between the single-vortex and the small vortex bundle pinning regimes. Below B_{sb}, in the low magnetic field region where the vortices are governed by single-vortex pinning, J_c is field independent. In this regime, $B_{sb} \propto J_{sv} B_{c2}$, where J_{sv} is the critical current density in the single-vortex regime. At higher fields, for $B > B_{sb}$, $J_c(B)$ decreases quickly, and it follows an exponential law, $J_c(B) \approx J_c(0) \exp[-(B/B_0)^{3/2}]$, where B_0 is a normalization parameter of the order of B_{sb}.

For clarification, $-\log[J_c(B)/J_c(0)]$ as a function of B is shown in a double-logarithmic plot in the inset of figure 3. It is clear that this expression describes well the experimental data for intermediate fields, while deviations from the fitting curve can be observed at both low and high fields. The deviation at low fields is associated with the crossover from single-vortex pinning regime to the small bundle pinning regime. The high field deviation that is very close to the irreversibility line could be related to large thermal fluctuations, a view that is supported by the three-dimensional (3D) flux creep dependence observed for the variation of $B_{irr}(T)$ in figure 1. The field of this deviation is denoted as B_{th}. The crossover field B_{sb} as a function of temperature is shown in figure 3. As a comparison, B_{sb} versus T for the undoped MgB_2 sample is also shown in the figure, and this plot displays a different trend from those of the doped samples.

It has been pointed out [25] that the δT_c and δl pinning mechanisms result in different temperature dependences of the critical current density J_{sv} in the single-vortex pinning regime. In this regime, the temperature dependence for B_{sb} is as $B_{sb}(T) = B_{sb}(0)\{(1 - t^2)/(1 + t^2)\}^{\nu}$, with $t = T/T_c$, where $\nu = 2/3$ and 2 for δT_c and δl pinning, respectively. We analyzed the B_{sb} data using the expression $B_{sb} = P_1 B_{sb}^{T_c} + P_2 B_{sb}^{l}$, with fitting parameters P_1 and P_2, where $B_{sb}^{T_c}$ and B_{sb}^{l} are the expressions for δT_c and δl pinning, respectively. The fitting results are shown in figure 3 by the dashed curves. In
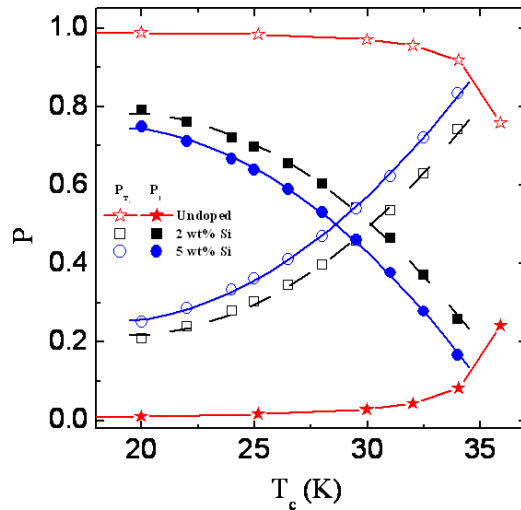
Figure 4. δT_c and δl pinning contributions as a function of temperature.

order to compare the contributions of the δT_c and δl pinning mechanisms, the P parameter is defined as $P = P_1 B_{sb}^{T_c}/B_{sb}$ or $P = P_2 B_{sb}^{l}/B_{sb}$, which represents the proportion of the contribution from δT_c or δl pinning, respectively.

The results of both pinning contributions are shown in figure 4. It can be seen that the δl and δT_c pinning mechanisms coexist in both the 2 and 5 wt% Si-added samples. The Mg deficiency in these samples leads to a broad distribution of T_c and thus is responsible for the δT_c pinning mechanism. At the same time, the fine particles of Mg_2Si cause the fluctuations in the mean free path that are responsible for the δl pinning. The δl and δT_c pinning mechanism contributions are strongly temperature dependent and show a strong competition. The δl pinning contribution is dominant at low temperatures, and it decreases with increasing temperature. The δT_c pinning shows the opposite trend. Between 28 and 30 K, the two pinning mechanisms have roughly equal effects, while above these temperatures, δT_c pinning is dominant. As can be seen from figure 4, for temperatures close to T_c, the T_c fluctuation among the grains increases, and therefore, the δl pinning is suppressed completely. When the temperature is far below T_c, the T_c fluctuation disappears, and the δl pinning is dominant. The two nano-Si-doped samples have the same trend in both the δl and δT_c pinning mechanisms. The slight difference in the proportions of the contributions is because the T_c is slightly different and the nano-Si inclusions are inhomogeneous in the two Si-doped samples. In contrast, the δT_c pinning is the dominating mechanism over the whole temperature range for the undoped MgB_2 sample, which is partially due to the Mg deficiency from the formation of MgO impurity phase, in agreement with our previous report [18].

In conclusion, we have found that the δl and δT_c pinning mechanisms coexist in the nano-Si-doped MgB_2 samples and that H_{c2} increases greatly with increasing nano-Si doping level. However, the relative contributions of the pinning mechanisms are strongly temperature dependent and show a strong competition. The δl pinning is dominant at low temperatures, decreases with increasing temperature, and is

suppressed completely at temperatures close to T_c. However, the δT_c pinning mechanism shows opposite trends.

References

[1] Bugoslavsky Y, Cohen L F, Perkins G K, Polichetti M, Tate T J, Gwilliam R and Caplin A D 2001 *Nature* **411** 561
[2] Liao X Z, Serquis A C, Zhu Y T, Huang J Y, Peterson D E, Mueller F M and Xu H F 2002 *Appl. Phys. Lett.* **80** 4398
[3] Eisterer M, Zehetmayer M, Tonies S, Weber H W, Kambara M, Babu N H, Cardwell D A and Greenwood L R 2002 *Supercond. Sci. Technol.* **15** L9
[4] Dou S X, Soltanian S, Horvat J, Wang X L, Zhou S H, Ionescu M, Liu H K, Munroe P and Tomsic M 2002 *Appl. Phys. Lett.* **81** 3419
[5] Dou S X, Yeoh W K, Horvat J and Ionescu M 2003 *Appl. Phys. Lett.* **83** 4996
[6] Ma Y W, Zhang X P, Nishijima G, Watanabe K, Awaji S and Bai X D 2006 *Appl. Phys. Lett.* **88** 072502
[7] Yamada H, Hirakawa M, Kumakura H and Kitaguchi H 2006 *Supercond. Sci. Technol.* **19** 179
[8] Wang X L, Zhou S H, Qin M J, Munroe P R, Soltanian S, Liu H K and Dou S X 2003 *Physica* C **385** 461
[9] Wang X L, Soltanian S, James M, Qin M J, Horvat J, Yao Q W, Liu H K and Dou S X 2004 *Physica* C **408–410** 63
[10] Karpinski J *et al* 2005 *Phys. Rev.* B **71** 174506
[11] Mudgel M, Chandra L S S, Ganesan V, Bhalla G, Kishan H and Awana V P S 2009 *J. Appl. Phys.* **106** 033904
[12] Vajpayee A, Awana V P S, Bhalla G L and Kishan H 2008 *Nanotechnology* **19** 125708
[13] Mudgel M, Awana V P S, Kishan H and Bhall G L 2008 *Solid State Commun.* **146** 330
[14] Larbalestier C *et al* 2001 *Nature* **410** 186
[15] Kim H J, Kang W N, Choi E M, Kim M S, Kim K H P and Lee S I 2001 *Phys. Rev. Lett.* **87** 087002
[16] Kim M S, Jung C U, Park M S D, Lee S Y, Kim K H P, Kang W N and Lee S I 2001 *Phys. Rev.* B **64** 012511
[17] Pallecchi I *et al* 2005 *Phys. Rev.* B **71** 212507
[18] Qin M J, Wang X L, Liu H K and Dou S X 2002 *Phys. Rev.* B **65** 132508
[19] Xu M, Kitazawa H, Takano Y, Ye J, Nishida K, Abe H, Matsushita A and Kido G 2001 *Appl. Phys. Lett.* **79** 2779
[20] Wang J, Shi Z X, Lv H and Tamegai T 2006 *Physica* C **445–448** 462
     Jung J, Isaac I and Mohamed M A K 1993 *Phys. Rev.* B **48** 7526
[21] Kim K H P *et al* 2002 *Phys. Rev.* B **65** 100510(R)
[22] Pradhan A K, Shi Z X, Tokunaga M, Tamegai T, Takano Y, Togano K, Kito H and Ihara H 2001 *Phys. Rev.* B **64** 212509
[23] Kazakov S M, Puzniak R, Rogacki K, Mironov A V, Zhigadlo N D, Jun J, Soltmann C, Batlogg B and Karpinski J 2005 *Phys. Rev.* B **71** 024533
[24] Dou S X *et al* 2007 *Phys. Rev. Lett.* **98** 097002
[25] Griessen R, Hai-hu W, van Dalen A J J, Dam B, Rector J and Schnack H G 1994 *Phys. Rev. Lett.* **72** 1910
[26] Blatter G, Feigel'man M V, Geshkenbein V B, Larkin A I and Vinokur V M 1994 *Rev. Mod. Phys.* **66** 1125
[27] Buzea C and Yamashita T 2001 *Supercond. Sci. Technol.* **14** R115
[28] Finnemore D K, Ostenson J E, Bud'ko S L, Lapertot G and Canfield P C 2001 *Phys. Rev. Lett.* **86** 2420
[29] Tarantini C *et al* 2006 *Phys. Rev.* B **73** 134518
[30] Wang J L, Zeng R, Kim J H, Lu L and Dou S X 2008 *Phys. Rev.* B **77** 174501